Supplementary information

Robust eutectic gel polymer electrolytes for high-performance zinc-ion batteries by solvent-exchange strategy

Zhengyang Zhu, Danyang Niu, Piaonan Chen, Yanchao Liang, Mengrui Wu, Jiayao Wang, Xin Yang, Lijun Ye, Jieqing Shen*, Yongjin Li*

College of Material, Chemistry and Chemical Engineering, Key Laboratory of Organosilicon Chemistry and Material Technology, Ministry of Education and Key Laboratory of Organosilicon Material Technology of Zhejiang Province, Hangzhou Normal University, 311121 Hangzhou, P. R. China

Zhejiang-South Africa Joint Laboratory of Sustainable Polymer Composite Materials and Technology, Hangzhou Normal University, Hangzhou 311121, P. R. China

*Corresponding authors

E-mail: jqshen@hznu.edu.cn (J. Shen), yongjin-li@hznu.edu.cn (Y. Li)

Experimental section

Materials. Polyvinyl alcohol (PVA, polymerization degree: 1799, 98-99% hydrolyzed), Aniline (99 %) and ammonium persulfate (99 %) were supplied by Aladdin. Dimethyl sulfoxide (DMSO), ethylene glycol (EG) and zinc perchlorate hexahydrate ($Zn(ClO_4)_2 \cdot 6H_2O$) were obtained from Sinopharm Chemical Regent Co., Ltd. All reagents were of analytical grade and used without further purification.

Preparation of DESs. (DESs) were prepared by mixing $Zn(ClO_4)_2 \cdot 6H_2O$ and EG at 90 °C with molar ratios of 1:2, 1:4, 1:6, 1:8, 1:10 and 1:12. The mixtures were stirred until homogeneous and transparent solutions were obtained.

Preparation of PVAx-DES EGPEs. PVA precursor solutions with concentrations of 15-35 w/v% were prepared by dissolving PVA1799 in DMSO at 90 °C under stirring for 3 h. Here, w/v% refers to the mass of PVA (g) per 100 mL of solvent; for example, dissolving 15 g of PVA in 100 mL of DMSO corresponds to a concentration of 15 w/v%. After defoaming, the precursor solution was cast onto a glass plate and kept at room temperature for 1 h before solvent exchange. The obtained films were then immersed in 500 mL of DES at room temperature for 24 h to induce solvent exchange, during which the DES bath was refreshed every 12 h to ensure sufficient solvent exchange. The obtained membranes were denoted as PVAx-DES, where x represents the PVA concentration in the precursor solution (x = 15, 20, 25, 30, 35 w/v%).

PANI cathode preparation. Aniline monomer (0.365 mL) was added to 15 mL of HCl (1.0 M) solution under stirring and the mixture was cooled to 0 °C in an ice bath. After stirring for 30 min, 5 mL of HCl (1.0 M) containing 0.228 g of ammonium

persulfate was added dropwise to the above solution. The initially colorless solution gradually turned dark green after a few minutes. After the reaction processed for 1 h, the resulting product (PANI) was washed with deionized water and ethanol and then dried at 60 °C. PANI based cathode was prepared by mixing PANI, acetylene black, and a binder (15 mg/mL polyvinylidene fluoride/*N*-methyl pyrrolidone) in a mass ratio of 5:4:1. The mixture was dispersed in isopropanol to form a slurry. After stirring for 5 h, the slurry was uniformly coated onto carbon cloth and then dried at 60 °C overnight. The average PANI loading was 0.95 mg/cm^2.

Preparation of V_2O_5 cathode. The commercialized V_2O_5, KB, and PVDF were mixed thoroughly with a mass ratio of 7:2:1 in 1 mL of *N*-methyl pyrrolidone (NMP) to obtain the uniformly dispersed slurry. The mixture was then pasted onto a graphite foil and dried at 60 °C in the vacuum oven for 24 h. The loading mass of V_2O_5 active material was about 1.1mg/cm^2.

Preparation of the pouch cell. Polyaniline (PANI), acetylene black, and binder were mixed in a mass ratio of 5:4:1 to prepare the cathode, with an average PANI loading of approximately 1 mg cm^{-2}. The cathode was cut into 5 × 5 cm^2 sheets after drying. The PVA30-DES gel electrolyte and Zn foil (50 μm) were cut into the same dimensions, and Ti foil was used as the current collector tab. The components were then assembled and laminated using aluminum plastic film, followed by vacuum sealing through hot pressing to obtain pouch cells.

Material characterizations. Fourier transform infrared (FTIR) spectra were recorded using a VERTEX 70v spectrometer (Bruker, Germany) with a resolution of 2

cm^{-1} and an accumulation of 64 scans. Nuclear magnetic resonance (NMR) spectra of the electrolytes were acquired on a Bruker Avance III 400 MHz spectrometer, using heavy water (D_2O) and as solvent and external references. The water content of the PVA30-DES was measured using Karl Fischer titration (KF Titrino plus) The morphology of cycled Zn anode was characterized by the scanning electron microscope (SEM, Sigma 500). The luminous transmittance (Tlum, 400-800 nm) spectra of EGPEs were collected by a dual beam spectrophotometer (Hitachi UH5300) at normal incidence. The 3D topographies of cycled Zn anode were obtained using atomic force microscopy (AFM, Bruker Dimension Icon). X-ray diffraction (XRD) measurements of EGPEs were carried out on a D8 Advance X-ray diffractometer (Bruker, Germany) with a scan rate of 2° min^{-1}. The XRD results were processed and fitted using the PeakFit software to determine the crystallinities of EGPEs. Thermogravimetric analysis (TGA) experiments were performed by TA Instruments Q500 under an air atmosphere with a heating rate of 10 °C min^{-1} over a temperature range from 30 to 800 °C. Tensile tests were performed using an Instron universal material testing system (model 5966) at a tensile rate of 10 mm min^{-1} at room temperature. Dumbbell-shaped samples were punched using a dumbbell-shaped cutter prior to mechanical testing.

To determine the polymer content of the EGPEs, the samples were first weighed, and the mass was recorded as m_1. The samples were then immersed in deionized water for 48 h to fully extract and remove the DES components. Afterward, the samples were dried at 80 °C for 6 h, and the final mass was recorded as m_2. The polymer content (W) was calculated according to the following equation:

$$W = \frac{m_2}{m_1} \times 100\%$$

Battery preparation and electrochemical tests. Cells with different configurations, including Zn//Zn, Zn//Cu, Zn//stainless steel (SS) and SS//SS, were assembled in CR2032 or CR2025-type coin cells to evaluate electrochemical performance. Unless otherwise specified, Zn anodes were 15 mm in diameter and 100 μm in thickness. The EGPEs, serving as electrolyte and separator, were cut into disks with a diameter of 19 mm. F or comparison, the electrochemical performance of the DES electrolyte was evaluated using a glass fiber separator (GF/A, Whatman) impregnated with 150 μL of DES.

The ionic conductivity of the electrolyte was measured by electrochemical impedance spectroscopy (EIS) using an AUTOLAB electrochemical workstation. Measurements were performed in symmetric SS//SS cells over a frequency range from 10^6 to 10^{-1} Hz with an AC amplitude of 10 mV at 25 °C. The ionic conductivity (σ) was calculated according to the following equation:

$$\sigma = \frac{L}{SR}$$

where L and S denote the thickness and effective area of the electrolyte membrane, respectively, and R represents the bulk resistance. Linear sweep voltammetry (LSV), Tafel plots, Chronoamperometry (CA) tests, and Cyclic voltammetry (CV) curves were performed using an AUTOLAB electrochemical workstation. CA tests were carried out using Zn//Zn cells at a constant potential of −150 mV. CV curves of the Zn//PANI cell with PVA30-DES were recorded within a potential window of 0.2-1.6 V at a scan rate of 1 mV s^{-1}. The long-term cycling performance of Zn//Zn, and Zn//PANI cells were

evaluated using a LANBTS battery testing system (BT-2018R), with Zn//PANI cells cycled within a voltage range of 0.5-1.5 V.

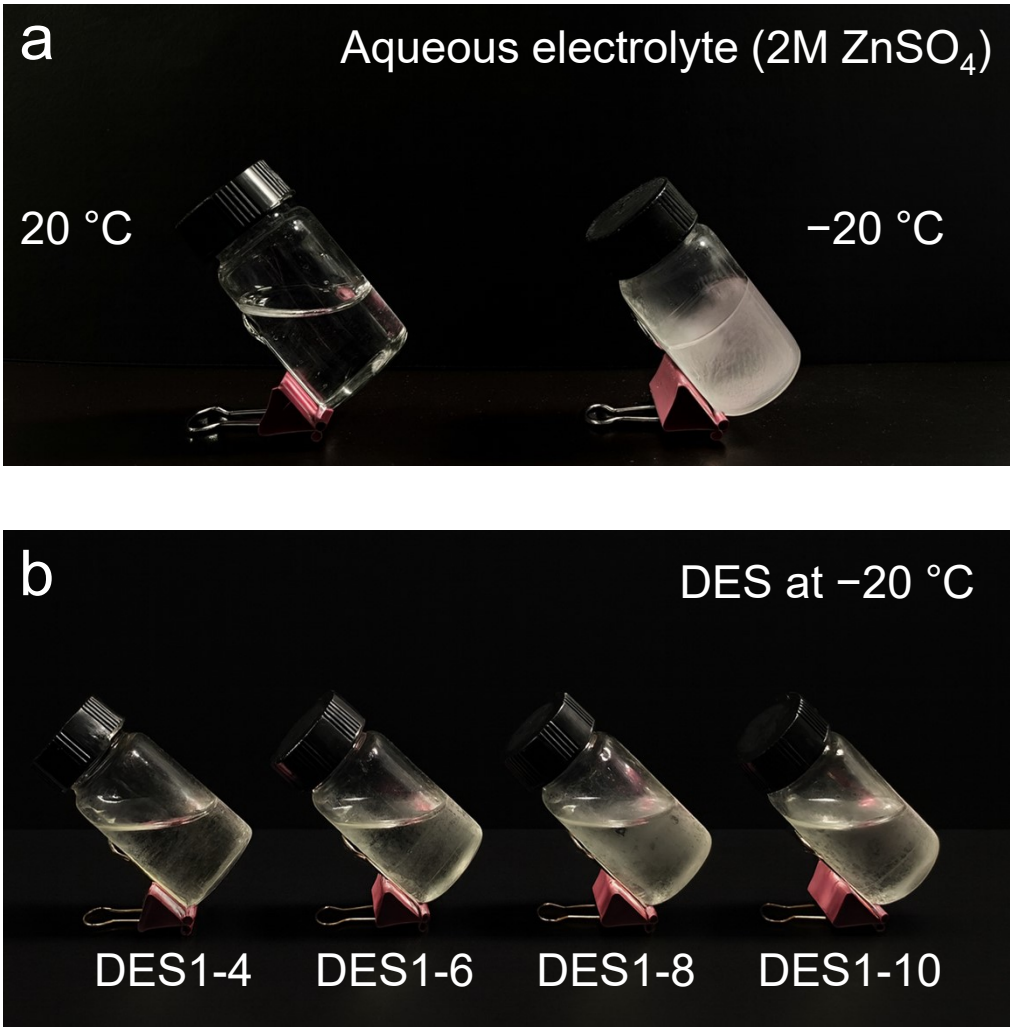

Fig. S1 Digital photos comparing the physical states of (a) the aqueous electrolyte (2 M $ZnSO_4$) and (b) the DES electrolyte at −20 °C.

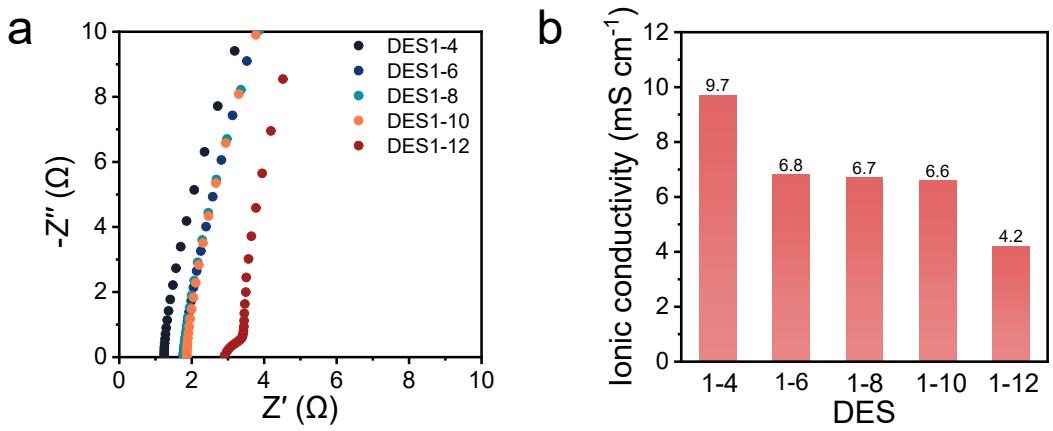

Fig. S2 (a) Electrochemical impedance spectroscopy of SS//SS cells with DES of different molar ratios. (b) Ion conductivity of DES with different molar ratios.

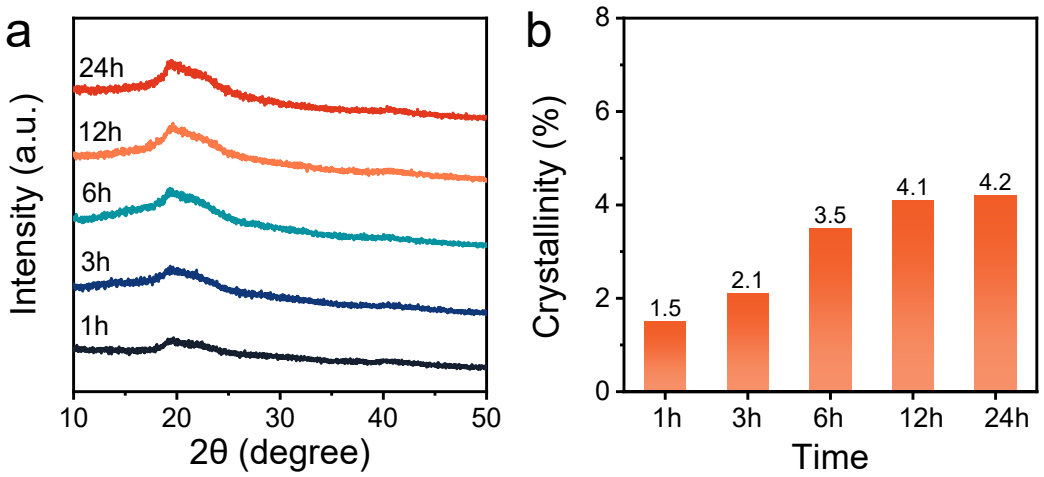

Fig. S3 (a) XRD patterns and (b) calculated crystallinities of PVA30-DES at different solvent exchange times.

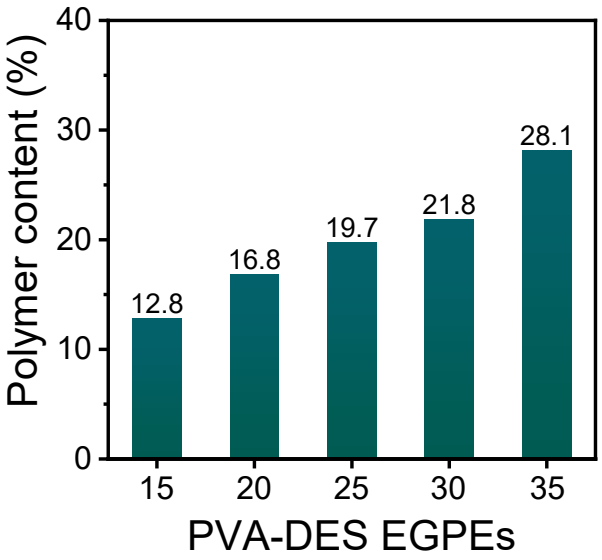

Fig. S4 Polymer content of PVA-DES EGPEs.

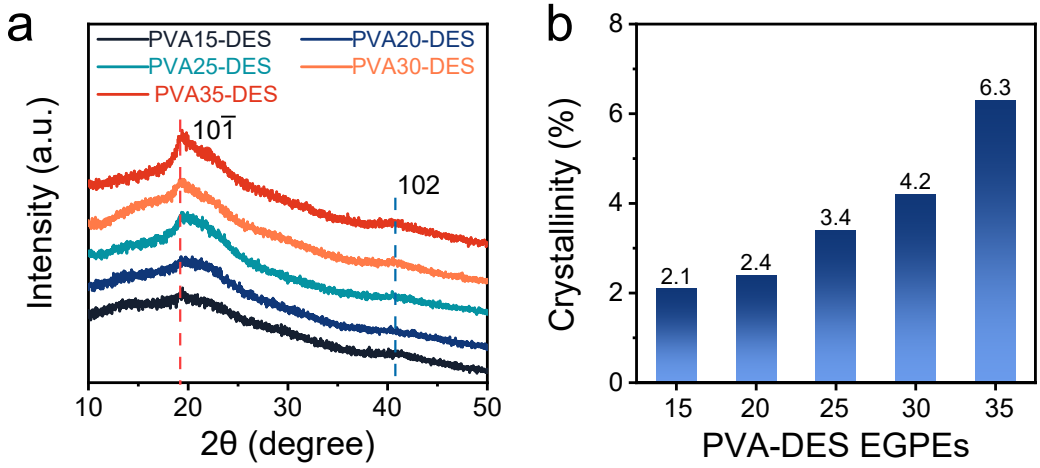

Fig. S5 (a) XRD patterns and (b) calculated crystallinities of PVA-DES EGPEs.

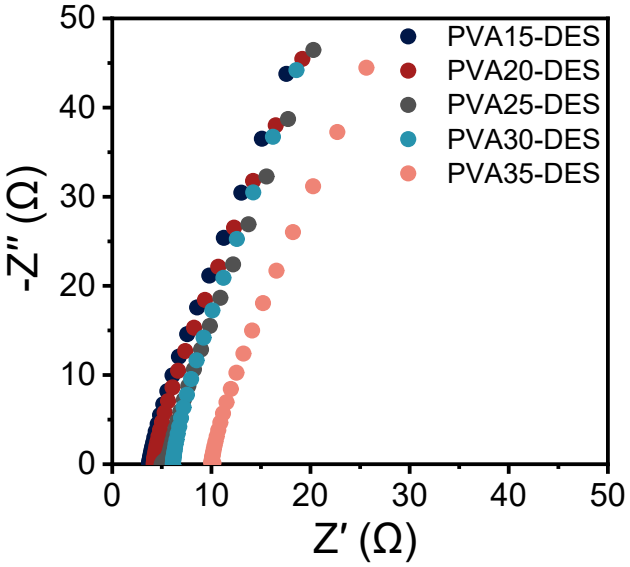

Fig. S6 EIS spectra of SS//SS cells with PVA-DES EGPEs.

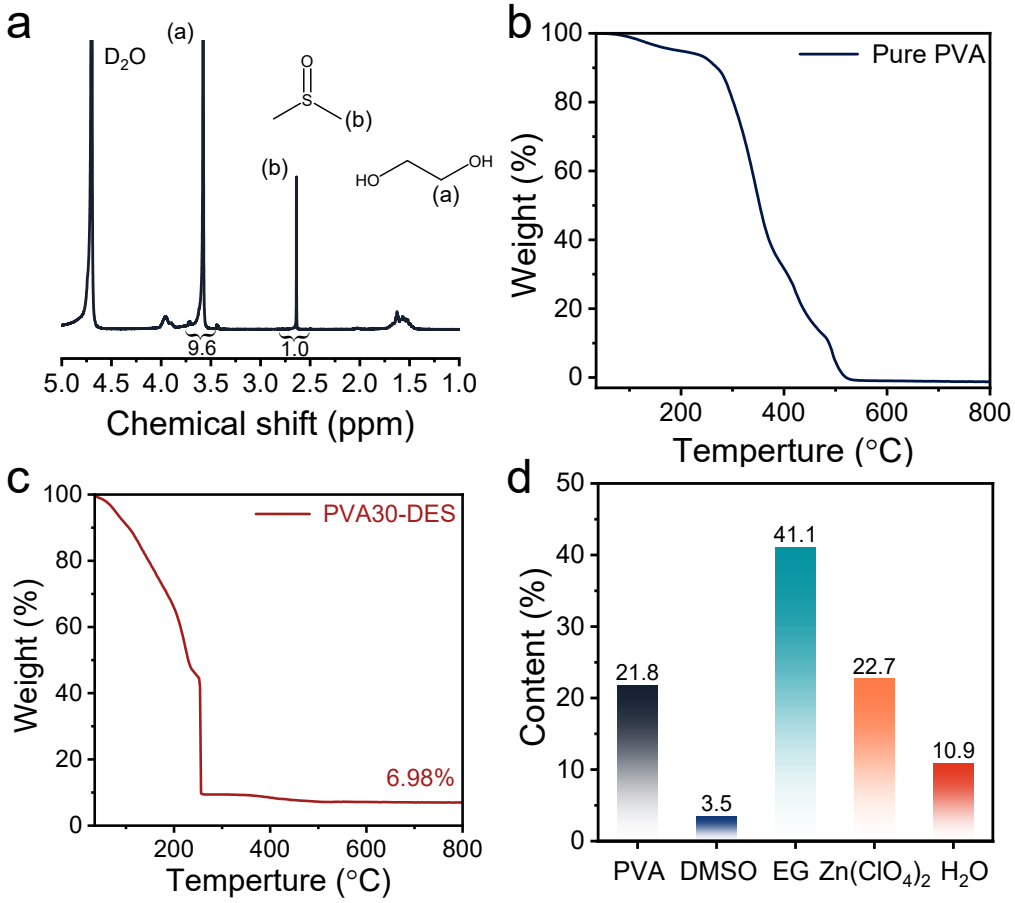

Fig. S7 (a) ^{1}H NMR spectra of PVA30-DES using D_2O as solvents. (b, c) TGA curves of (b) pure PVA and (c) PVA30-DES measured from 30 to 800 °C. (d) Composition of PVA30-DES.

To clarify the complete composition of the PVA30-DES EGPE. A multi-step analytical approach was employed using ^{1}H NMR spectroscopy, Karl Fischer titration and TGA. Initially, quantitative ^{1}H NMR spectroscopy was used to evaluate the relative mass ratio of the liquid components (**Fig. S7a**).[1] By analyzing the integral area ratios of the methylene protons of EG to the methyl protons of DMSO (9.6:1), the mass ratios of EG and DMSO were calculated. Concurrently, the inorganic salt content was quantified by TGA (**Fig. S7b** and **S7c**). While pure PVA showed complete thermal decomposition, the PVA30-DES electrolyte yielded a final residual mass of 6.98%,

corresponding to the formation of ZnO derived from zinc perchlorate ($Zn(ClO_4)_2$). This result enabled the back-calculation of the $Zn(ClO_4)_2$ content, which was determined to be 22.7%. the water content of the eutectic gel polymer electrolyte was determined using Karl Fischer titration, which is a more accurate and widely accepted method for water quantification.[2] The average water content was measured to be 10.9%. By combining the NMR and TGA results with the obtained PVA mass fraction (**Fig. S7**), the composition of the PVA30-DES electrolyte was determined to be PVA (21.8%), EG (41.1%), H_2O (10.9%), DMSO (3.5%), and $Zn(ClO_4)_2$ (22.7%).

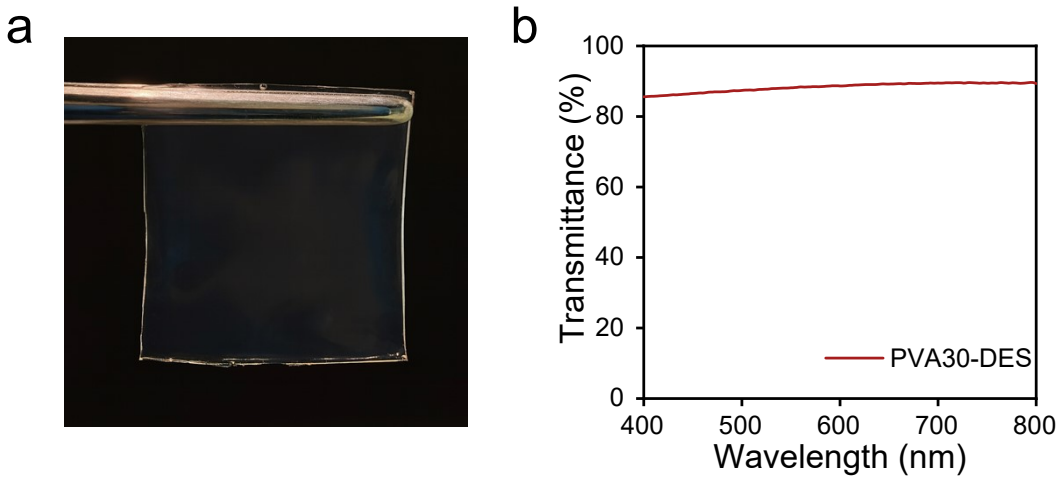

Fig. S8 (a) Digital photo of PVA30-DES. (b) Transmittance spectra of PVA30-DES.

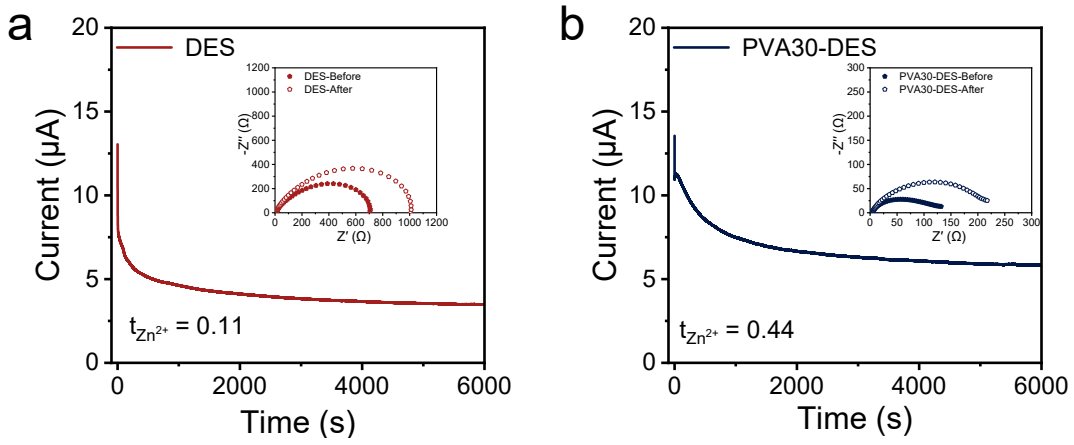

Fig. S9 Variation of current with time during polarization for Zn//Zn cells with (a) DES and (b) PVA30-DES. Inset: EIS spectra of Zn//Zn cells with different electrolyte before and after polarization.

Zn^{2+} transference number ($t_{Zn^{2+}}$) were evaluated using symmetric Zn cells by combining EIS measurements conducted before and after CA tests. The $t_{Zn^{2+}}$ of electrolyte is calculated according to the following equation:

$$t_{Zn^{2+}} = \frac{I_s(\Delta V - I_0 R_0)}{I_0(\Delta V - I_s R_s)}$$

Where ΔV represents the applied overpotential (20 mV), I_s and R_s are the steady state current and resistance, respectively, I_0 and R_0 correspond to the initial current and resistance, respectively.

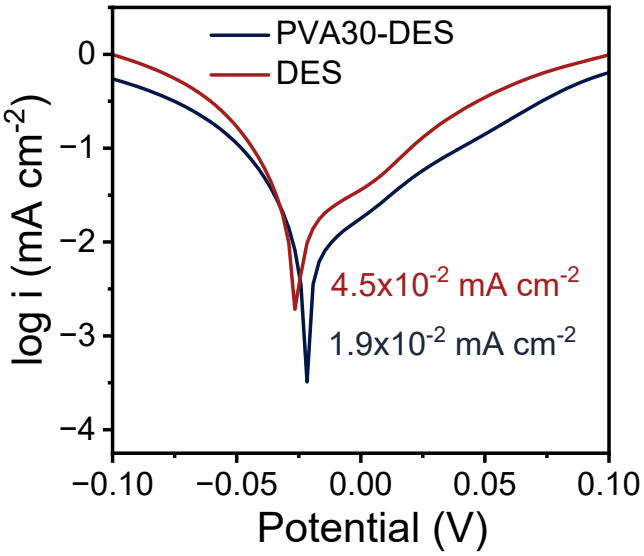

Fig. S10 Tafel plots of Zn//Zn cells with PVA30-DES and DES electrolytes.

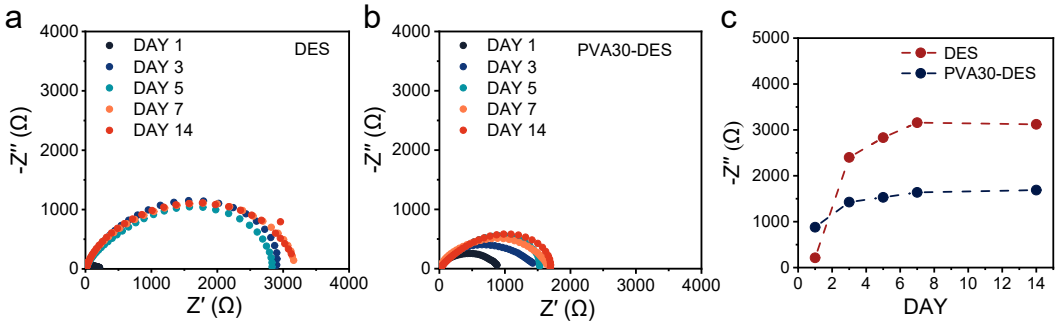

Fig. S11 EIS of Zn//Zn cells with (a) DES and (b) PVA30-DES after resting for 1, 3, 5, 7, and 14 days. (c) Comparison of the interfacial impedance evolution for Zn//Zn cells with DES and PVA30-DES.

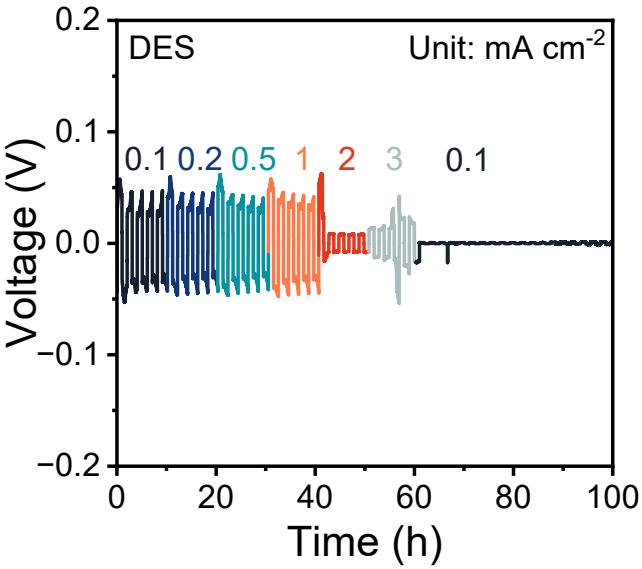

Fig. S12 Rate performance of Zn//Zn cell with DES electrolyte at current densities of 0.1-3 mA cm^{-2}.

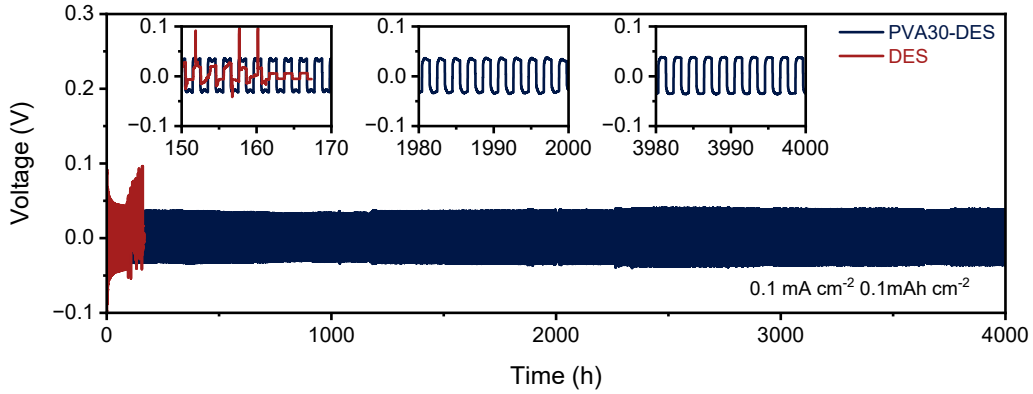

Fig. S13 Galvanostatic charge/discharge performance of Zn//Zn cells with DES and PVA30-DES at 0.1 mA cm^{-2}, 0.1 mAh cm^{-2}.

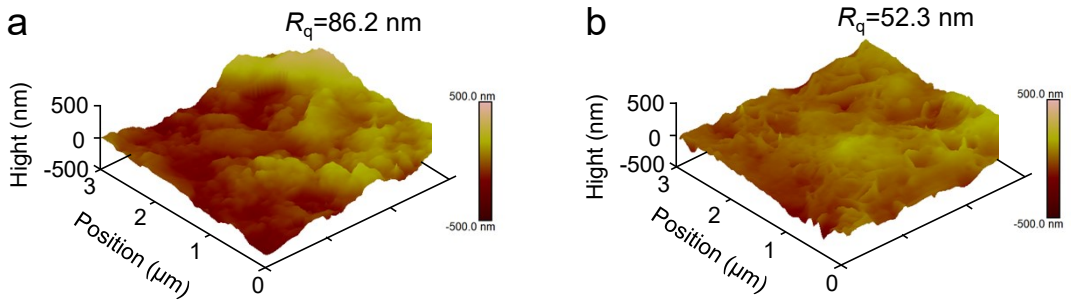

Fig. S14 AFM images of cycled Zn anodes detached from symmetric Zn cells with (a) DES and (b) PVA30-DES electrolyte.

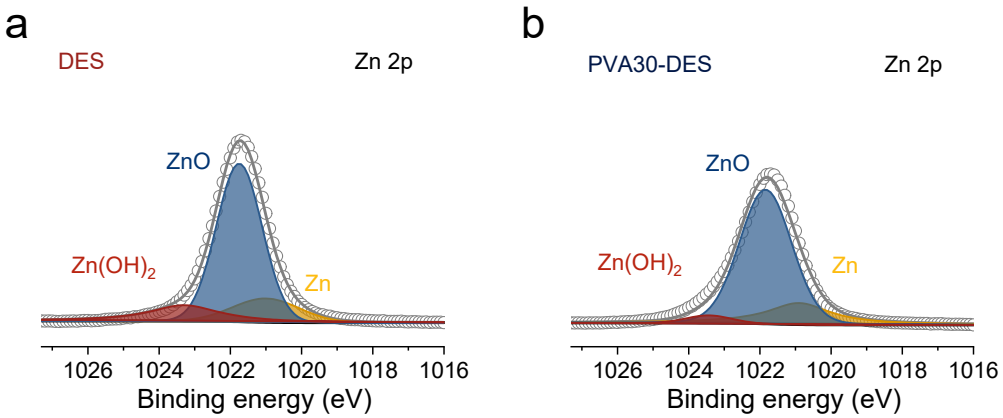

Fig. S15 Zn 2p XPS spectra of the cycled Zn anode detached from Zn//Zn cells cycled with (a) DES and (b) PVA30-DES electrolyte.

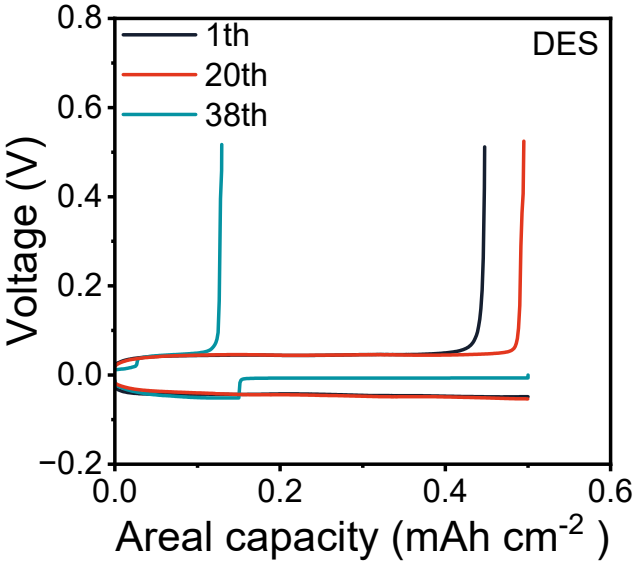

Fig.S16 Voltage profiles of Zn//Cu cell with DES electrolyte cycled at 0.5 mA cm^{-2}, 0.5 mAh cm^{-2}.

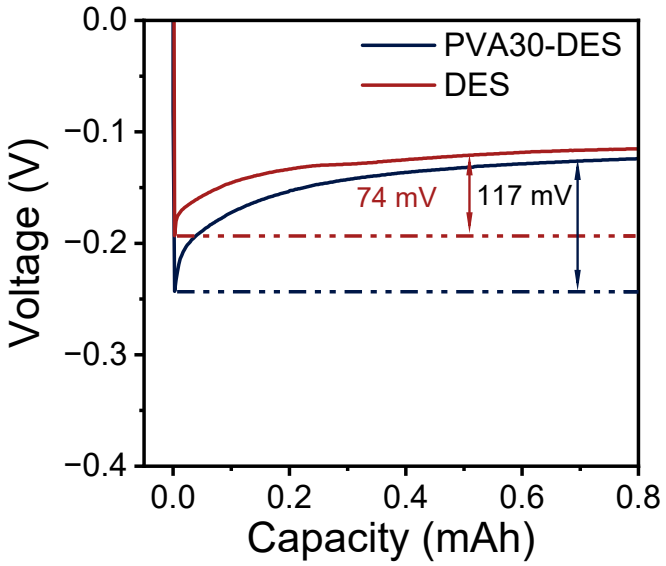

Fig. S17 Nucleation overpotential curves for Zn nucleation at the Cu electrode in DES and PVA30-DES systems.

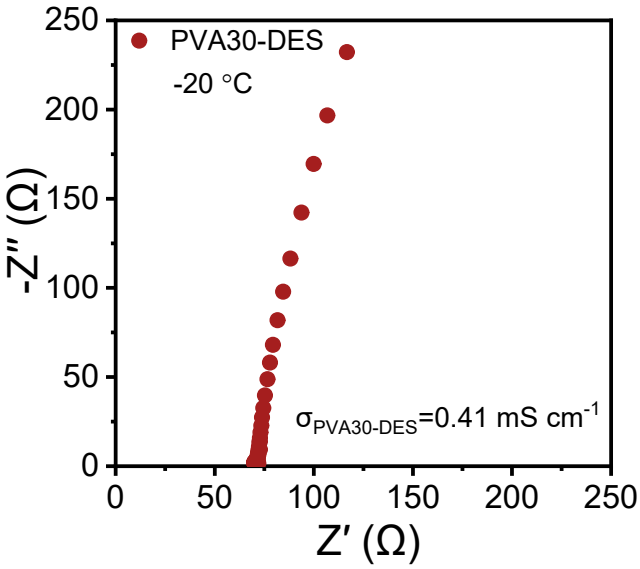

Fig. S18 EIS spectra of SS/SS cell with PVA30-DES electrolyte and ionic conductivity of PVA30-DES at −20 °C.

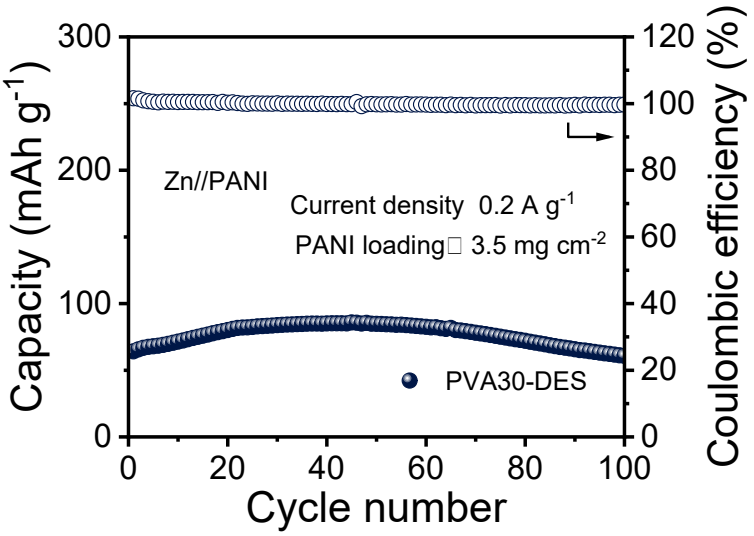

Fig. S19 Cycling performance of Zn//PANI cell with PVA30-DES under high mass loading at 0.2 A g^{-1}.

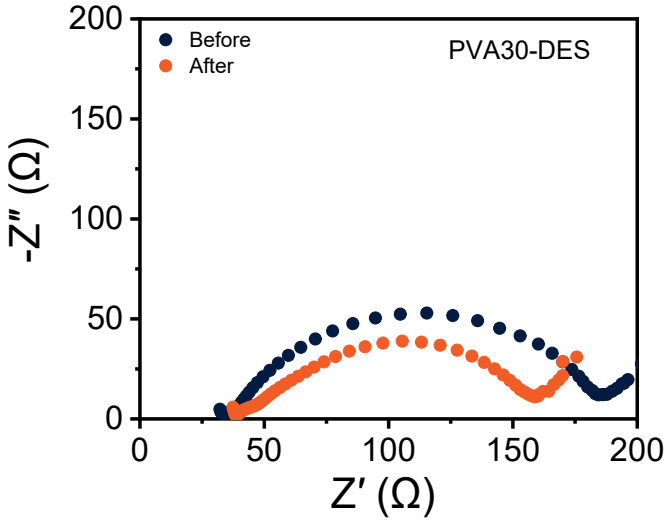

Fig. S20 EIS plots of Zn//PANI cell with PVA30-DES electrolyte before and after cycling.

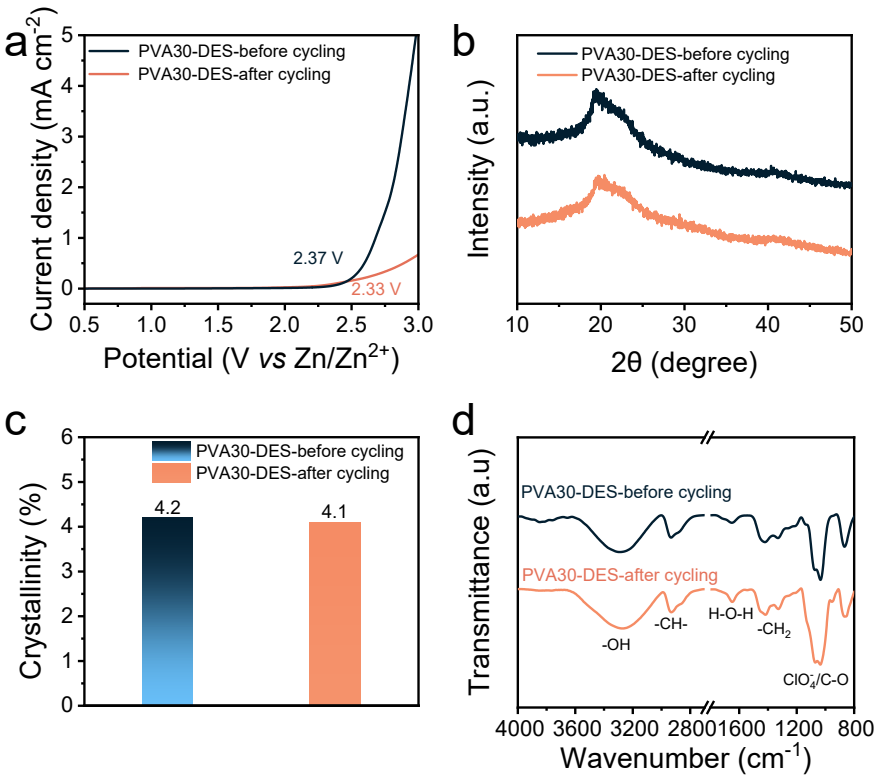

Fig. S21 (a) LSV curves of PVA30-DES before and after cycling. (b) XRD patterns of PVA30-DES electrolyte before and after cycling, and (c) the calculated crystallinities. (d) FTIR spectra of PVA30-DES before and after cycling.

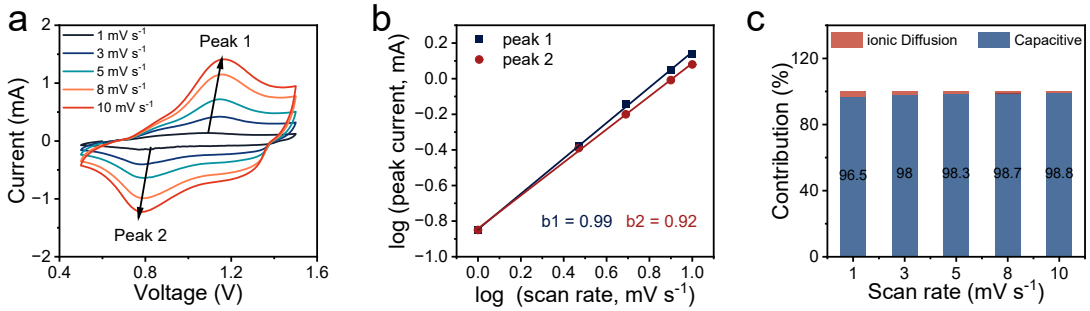

Fig. S22 (a) CV curves of the Zn//PANI battery with PVA30-DES at the scan rates from 1 to 10mV s^{-1}. (b) The corresponding log (peak current) versus log (scan rate) plots. (c) The capacitive and ionic diffusion contribution at different scan rates.

The redox reaction kinetics of PANI cathode in PVA30-DES systems were investigated. CV tests of Zn//PANI cell with PVA30-DES electrolyte were conducted at scan rates ranging from 1 to 10 mV s^{-1} (**Fig. S22a)**. The relationship between peak current (i) and sweep rate (v) can be fitted to this phenomenological model

$$i = av^b$$

where *a* and *b* are adjustable parameters. In particular, the *b* value serves as an indicator of the charge storage mechanism, with values close to 0.5 indicating a diffusion-controlled Faradaic process, while values close to 1 indicating a capacitive process.[3, 4] Based on the redox peaks, *b* values of 0.99 and 0.92 for peak 1 and peak 2 were obtained, respectively (**Fig. S22b**), suggesting that the charge/discharge process of the Zn//PANI cell with PVA30-DES is predominantly governed by pseudocapacitive behavior.

The capacity contributions of the PANI were deconvoluted according to $i = k_1 v + k_2 v^{1/2}$, where $k_1 v$ represents the capacitive and $k_2 v^{1/2}$ corresponds to diffusion-controlled processes, respectively.[5] As shown in **Fig. S22c**, the capacitive

contribution increased markedly with increasing scan rate and reached 98.8% at 10 mV s^{-1}, confirming the dominant pseudocapacitive nature of the PANI cathode in the PVA30-DES system.[6]

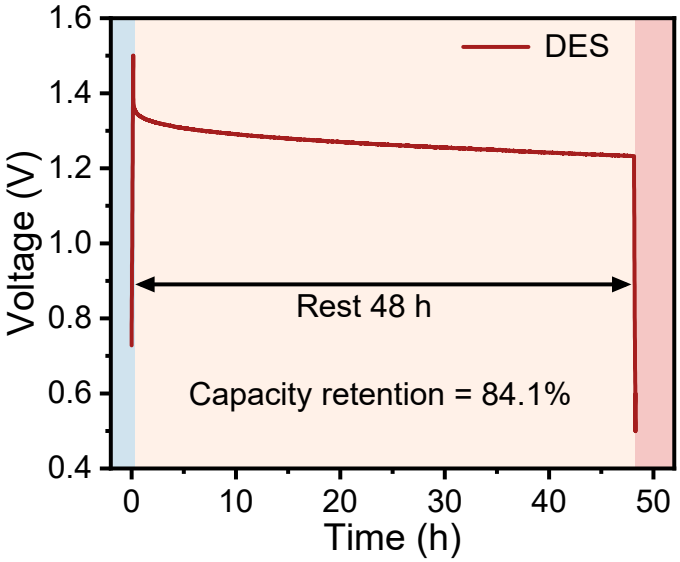

Fig. S23 Self-discharge test of Zn//PANI cell using DES electrolyte after 48 h rest.

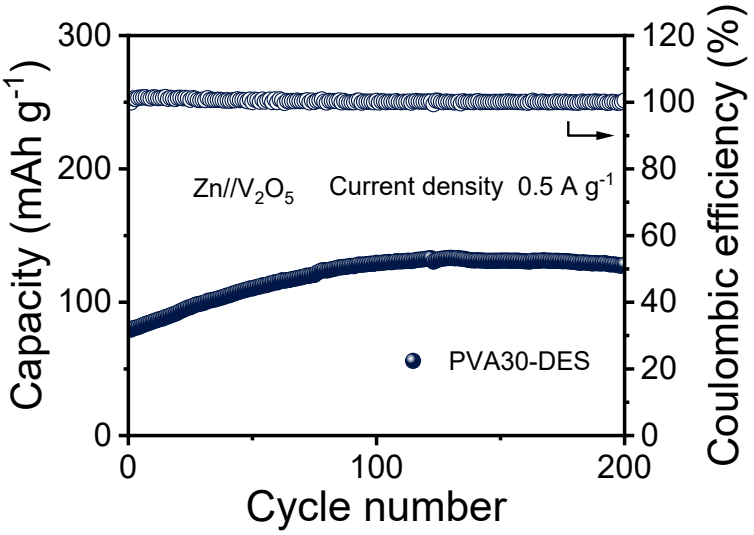

Fig. S24 Cycling performance of $Zn//V_2O_5$ cell with PVA30-DES electrolytes cycled at 0.5 A g^{-1}.

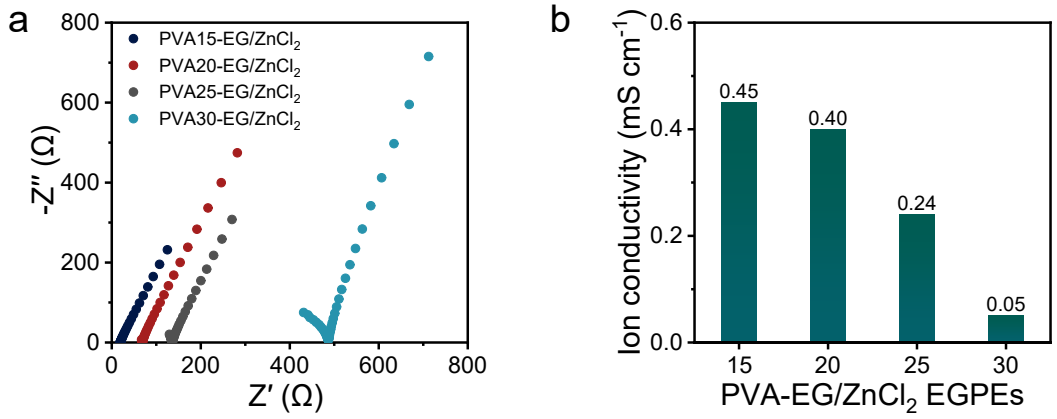

Fig. S25 (a) EIS results of SS//SS cells with PVA-EG/$ZnCl_2$ EGPEs and (b) ion conductivities of the PVA-EG/$ZnCl_2$ EGPEs.

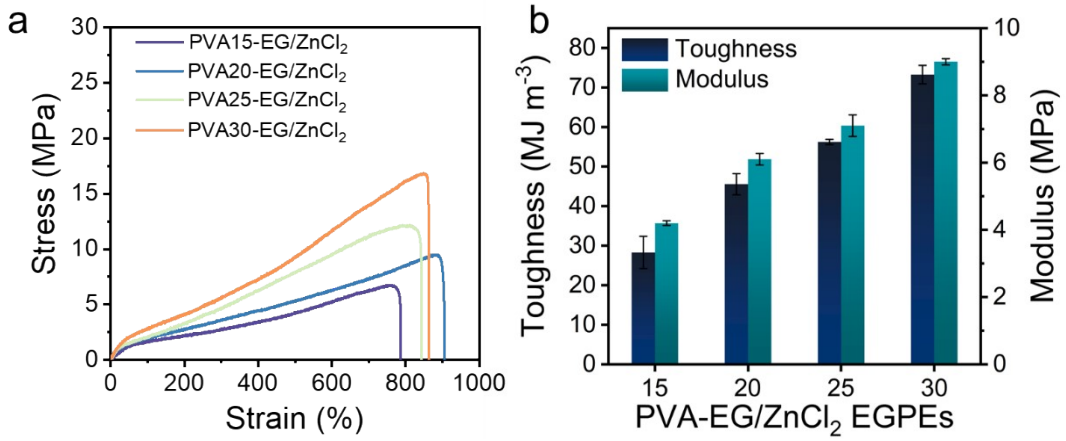

Fig. S26 (a) Stress-strain curves, and (b) the corresponding modulus and toughness values of the PVA-EG/$ZnCl_2$ EGPEs.

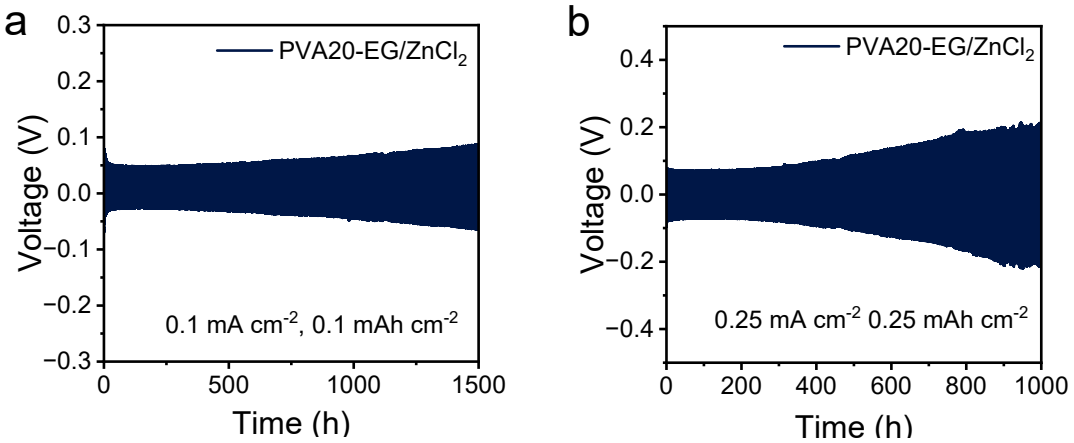

Fig. S27 Voltage profiles of Zn//Zn batteries with PVA20-EG/$ZnCl_2$ EGPEs at current densities of (a) 0.1 mA cm^{-2}, 0.1 mAh cm^{-2} and (b) 0.25 mA cm^{-2}, 0.25 mAh cm^{-2}.

Table S1. Comparison of the properties of the PVA30-DES EGPE proposed in this work with recently reported results.

Reported GPE	Tensile strength (MPa)	Toughness (MJ m^{-3})	Young's modulus (MPa)	Ionic conductivity (mS cm^{-1})	Low-temperature cycling temperature (°C)	Ref.
*PVA30-DES	8.10	58.11	5.10	5.20	−20 °C	This work
*DA-ETG	0.60	0.03	0.76	0.33	−20 °C	7
*PAA-DES	0.06	0.10	0.02	1.52	−60 °C	8
*$PD_{1.5}EM_{0.3}$	0.02	0.23	0.01	16.8	−20 °C	9
*PZE4-W	0.74	0.21	0.15	4.55	−35 °C	10
*DGel-$Fe_2L_{0.5}$	1.75	0.85	0.17	0.60	−20 °C	11
*P(AA-co-VIPS)	0.18	0.16	0.06	3.10	−20 °C	12
#PDHE	2.20	0.24	0.98	17.7	25 °C	13
#PCG20–PC5	0.43	0.08	0.30	16.18	25 °C	14

*: eutectic gel polymer electrolyte. #: hydrogel polymer electrolyte

As shown in **Table S1**, the PVA30-DES exhibits an ionic conductivity of 5.20 mS cm^{-1}, together with robust mechanical properties, including high Young's modulus of 5.10 MPa and high toughness of 58.11 MJ m^{-3}. These values compare favorably with representative gel polymer electrolytes summarized in **Table S1**, which typically exhibit a trade-off between ionic conductivity and mechanical robustness. High ionic conductivity is often achieved at the expense of poor mechanical stability, while improving mechanical properties usually leads to reduced ionic conductivity.[15-17] Therefore, the PVA30-DES EGPE simultaneously maintains a practically useful ionic conductivity while exhibiting robust mechanical properties, thereby breaking this trade-off between mechanical reliability and ion transport. In addition, we further compared the reported operating temperatures of batteries employing different gel polymer

electrolyte systems in the literatures.[7-14] As summarized in **Table S1**, batteries based on deep eutectic electrolytes can typically operate at temperatures below −20 °C, whereas hydrogel-based electrolyte systems are usually limited to near-room-temperature operation due to the relatively high freezing point of water. These results further highlight the advantage of the EGPEs system presented in this work, which enables stable electrochemical cycling at low temperatures, demonstrating its potential for practical applications under subzero conditions.

Table S2. Comparison of the ionic conductivity of the PVA30-DES electrolyte proposed in this work with other GPEs for zinc batteries.

Reported GPE	Ionic conductivity (mS cm^{-1})	Temperature (°C)	Ref.
*PVA30-DES	0.41	−20 °C	This work
*DA-ETG	0.29	−20 °C	7
*DGel-$Fe_2L_{0.5}$	0.09	−20 °C	11
*P(AA-co-VIPS)	0.08	−20 °C	12
#Lig/SPI-50%	0.02	−20 °C	20
#AP mono-salt	2.00	−20 °C	21
#MAANa/DMC-5 wt%	0.03	−20 °C	22

*: eutectic gel polymer electrolyte. #: hydrogel polymer electrolyte

References

1 N. R. Babij, E. O. McCusker, G. T. Whiteker, B. Canturk, N. Choy, L. C. Creemer, C. V. D. Amicis, N. M. Hewlett, P. L. Johnson, J. A. Knobelsdorf, F. Li, B. A. Lorsbach, B. M. Nugent, S. J. Ryan, M. R. Smith and Q. Yang, *Org. Process Res. Dev.*, 2016, **20**, 661-667.

2 B. Jadach, M. Misek and J. Ferlak, *Gels*, 2023, **9**, 687.

3 W. Wei, X. Feng, R. Wang, R. Zheng, D. Yang and H. Chen, *Nano Lett.*, 2021, **21**, 4830-4837.

4 V. Augustyn, J. Come, M. A. Lowe, J. W. Kim, P.-L. Taberna, S. H. Tolbert, H. D. Abruña, P. Simon and B. Dunn, *Nat. Mater.*, 2013, **12**, 518-522.

5 F. Huang, Y. Guo, W. Zhao, R. Wu, Y. Dong, G. Long and P. Du, *Chem. Eng. J.*, 2024, **498**, 155248.

6 D. Feng, Y. Jiao and P. Wu, *Angew. Chem. Int. Ed.*, 2023, **62**, e202215060.

7 X. Li, Z. Li, Z. Guo, C. Zhang, X. Xu, J. Tu, X. Wang and C. Gu, *ACS Appl. Mater. Interfaces*, 2024, **16**, 36901-36910.

8 X. Liu, J. Wang, P. Lv, Y. Zhang, J. Li and Q. Wei, *Energy Storage Mater.*, 2024, **69**, 103382.

9 T. Li, J. Liu, H. Shu, A. Sun, T. Zhao, Y. Chen and Y. Chen, *Adv. Funct. Mater.*, 2025, DOI: https://doi.org/10.1002/adfm.202514358, e14358.

10 Q. Peng, R. Cao, H. Ma, Y. Li, E. Zhu, X. Zhu, N. Ma, M. Xue and X. Zhang, *J. Mater. Chem. A*, 2025, **13**, 6586-6596.

11 J. Wang, Y. Deng, Z. Ma, Y. Wang, S. Zhang and L. Yan, *Green Chem.*, 2021, **23**, 5120-5128.

12 X. Bu, Y. Ge, L. Wang, L. Wu, X. Ma and D. Lu, *Polym. Eng. Sci.*, 2021, **61**, 154-166.

13 Q. He, Y. Zhong, J. Li, S. Chai, Y. Yang, S. Liang, Z. Chang, G. Fang and A. Pan, *Adv. Energy Mater.*, 2024, **14**, 2400170.

14 Q. Wang, J. Huang, L. Qi, M. Li, S. Wang, J. Chen, Z. Sui, T. Bi, Q. Tang, L. Yu, P. Hu, W. Zhang, C. Lu and C. Chen, *ACS Nano*, 2025, **19**, 26770-26781.

15 X. Yan, J. Zhang, Y. Sheng, K. Chen, H. Zhao, Q. Zhang, Y. Cheng, Z. Ge, X. Ming and Y. Zhang, *ACS Nano*, 2025, **19**, 40579-40593.

16 H. Wang, J. Yang, X. Xu, J. Geng, X. Lin, H. Xu and Y. Huang, *Adv. Mater.*, 2025, **37**, e04625.

17 J. Shen, W. Tian, S. Liu, H. Pan, C. Yang, H. Quan and S. Zhu, *ACS Nano*, 2024, **18**, 30716-30727.

18 B. Zhu, Y. Yan, J. Hong, Y. Xia, M. Song, X. Wang, Y. Liu, B. Zhong, D. Liu, T. Zhang and X. Huang, *J. Energy Chem.*, 2025, **109**, 325-336.

19 J. Wang, K. Zhao, Y. Zhao and C. Ye, *Small*, 2025, **21**, 2410806.

20 Y. Duan, J. Long, Y. Li, X. Tian, J. Li, Z. Fang, J. Wang and P. Huo, *J. Solid State Electrochem.*, 2024, **28**, 2021-2033.

21 N. Chelfouh, G. Coquil, S. Rousselot, G. Foran, E. Briqueleur, F. Shoghi, L. Caradant and M. Dollé, *ACS Sustainable Chem. Eng.*, 2022, **10**, 15802-15812.

22 X. Li, L. Kong and G. Gao, *J. Mater. Chem. B*, 2021, **9**, 2010-2015.